Fast-electron production in atomic collisions induced by 77*A*-MeV ^{40}Ar ions studied with a multidetector

G. Lanzanò, E. De Filippo, S. Aiello, M. Geraci, and A. Pagano
Instituto Nazionale di Fisica Nucleare and Dipartimento di Fisica, Corso Italia 57, 95129 Catania, Italy

Sl. Cavallaro and F. Lo Piano
Instituto Nazionale di Fisica Nucleare, Laboratorio Nazionale del Sud, and Dipartimento di Fisica, Corso Italia 57, 95129 Catania, Italy

E. C. Pollacco, C. Volant, and S. Vuillier
DAPNIA, Service de Physique Nucléaire, Commissariat à l'Energie Atomique de Saclay, F-91191 Gif-sur-Yvette Cedex, France

C. Beck, D. Mahboub, and R. Nouicer
IReS and Université L. Pasteur, F-67037 Strasbourg, France

G. Politi
Grand Accélérateur National d'Ions Lourds, Boîte Postale 5027, 14021 Caen Cedex, France

H. Rothard
Interdisciplinaire de Recherches avec les Ions Lourds (CIRIL), CEA-CNRS, UMRII, Boîte Postale 5133, F-14070 Caen Cedex 05, France

D. H. Jakubassa-Amundsen
Physics Section, University of Munich, D-85748 Garching, Germany
(Received 17 December 1997)

Fast electron velocity spectra have been measured by means of the multidetector ARGOS (actually located at Laboratorio Nazionale del Sud, Catania) in a large angular range for atomic collisions induced by a 77*A*-MeV ^{40}Ar beam on an Al target. The results are in a fair agreement with a recently proposed relativistic billiard ball model and quasielastic scattering approximation calculations. However, the experimental binary-encounter peak velocities are found to be significantly lower than theoretically predicted. The data also show evidence for an excess of fast electrons in the backward direction. [S1050-2947(98)06310-0]

PACS number(s): 34.50.Fa, 25.70.−z, 79.20.Rf

I. INTRODUCTION

It is well known to experimental nuclear physicists that a great number of fast electrons are produced when an ion beam of intermediate energy ($\approx 20A$ MeV$< E <200A$ MeV) impinges on a solid foil target. They are in general a source of disturbance for experimental detection systems, affecting their resolution. To avoid this inconvenience, it is customary to apply a suitably high voltage on the target holder or to use magnetic deflectors. No systematic experimental investigations, however, have been carried out on this field. From an atomic collision physics point of view, studies at beam energies above 10*A* MeV are quite scarce (for reviews see, e.g., [1–3]). Only recently, fast electron energy spectra have been the object of particular studies by solid state experimentalists or atomic collision theorists [1,4–7].

From these studies, it emerges that in the forward beam direction, fast electrons are essentially due to two reaction mechanisms. A binary encounter (BE) between the incident ion and an atomic electron produces electrons with a maximum velocity of almost twice the projectile velocity. Also, target electrons may be captured or projectile electrons may be lost into low-lying projectile centered continuum states. These so-called convoy electrons travel with a velocity close to that of the projectile and lead to a cusp-shaped peak in electron spectra. Electrons of velocity higher than the one corresponding to the binary encounter have also been observed and explained as due to multiple scattering within the combined target-projectile system [8,9]. The observation of energetic electrons at large angles and even in the backward direction have been explained in part by transport theories [1,4,10].

In the following, after a short description of the ARGOS multidetector array, the experimental results will be presented and compared with the predictions of the simple model of Ref. [5] and the calculations of Ref. [6].

II. EXPERIMENTAL SETUP AND DETECTION METHOD

The experiment was done at GANIL using a 77*A*-MeV 18^+ ^{40}Ar beam impinging on a 90-μg/cm^2-thick Al target, tilted at 45° with respect to the beam direction. The ARGOS multidetector [11] was placed in the large scattering chamber NAUTILUS. Depending on the experimental requirements, the ARGOS detectors can be arranged in various arrays.

Each detector consists of a hexagonal BaF_2 crystal modified into phoswich by means of a fast plastic scintillator sheet of suitable thickness, according to the charge and dy-

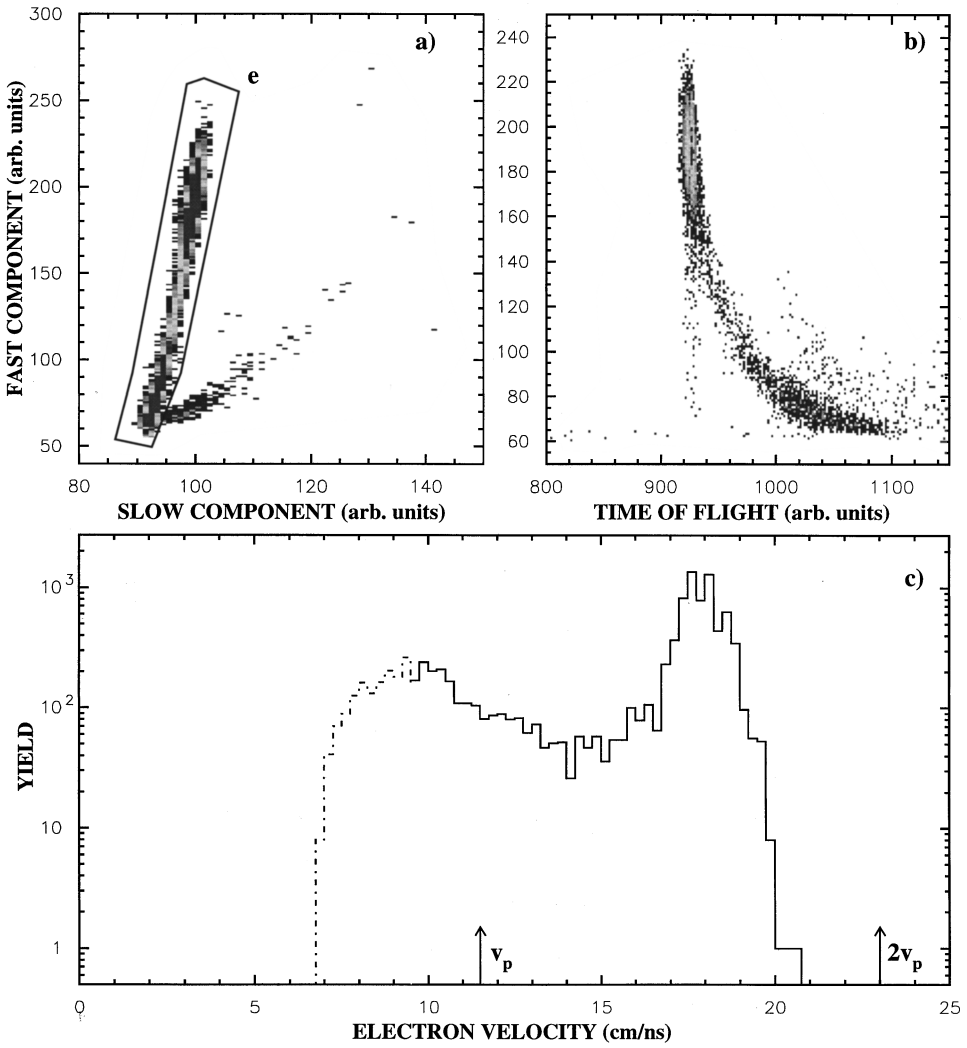

FIG. 1. Two-dimensional plot of the fast PM signal component as a function of (a) the slow component and (b) the time of flight, respectively, from the reaction ^{40}Ar ($77A$ MeV)$+^{27}$Al for a detector placed at $-10°$ with the PM gain increased in order to optimize the electron detection. (b) shows the fast component as a function of the time of flight for electrons selected by the contour plot indicated by e in (a). The corresponding velocity spectrum, obtained by taking as a reference the prompt γ-ray peak, is shown in the histogram of (c). The part of the histogram affected by threshold effects is represented by a dash-dotted line. The beam velocity ($v_P = 11.5$ cm/ns) and twice the beam velocity ($2v_P = 23$ cm/ns) are indicated.

namical range of the ions to be detected [11–13]. The light created by the particles is collected by photomultipliers (PM's). Each crystal has a surface of 25 cm^2 and a thickness variable up to 10 cm, stopping protons of energy up to 200 MeV. In addition to energetic photons, this phoswich detector can identify light charged particles, heavy ions, and even neutrons (with an efficiency of about 8% [14]). A full detection of electrons involves a substantial increase of the PM voltage, so the PM electronic pulses overcome the discriminator electronic thresholds and hence can be properly processed by the QDC (charge to digital converter). This implies the saturation of PM signals for energetic particles. Timing characteristics of the phoswich detector are well enhanced, reaching values less than about 250-ps resolution, so that precise time-of-flight measurements are possible if suitable flight paths and start signals with good time resolution are available. The ARGOS detector array is described in more detail in Refs. [11–13, 15,16].

The present arrangement consisted of three distinct parts: (i) a forward wall of 60 phoswiches, placed between 0.7° and 7° with a honeycomb shape at a distance of 235 cm from the target, with an angular separation between the centers of two adjacent detectors of approximately 1.5°; (ii) a backward wall of 18 phoswiches, placed between 160° and 175° at a distance of 50 cm from the target; and (iii) a battery of approximately 30 detectors in the horizontal plane, on both sides of the beam direction, between 10° and 150° and at a distance from the target varying from 2 to 0.5 m according to the expected counting rate. In the following, negative angles will be adopted for the detectors lying on the same side as the one affected by the target shadow at 45°. Also, in the backward direction there is a target shadow at 135° for positive angles. A particle produced in a nuclear or atomic reaction will have to cross a thicker target in the forward angular range when emerging at negative angles than in the case of corresponding positive angles. The geometry is shown in the inset of Fig. 4.

In this experiment we used a plastic scintillator thickness

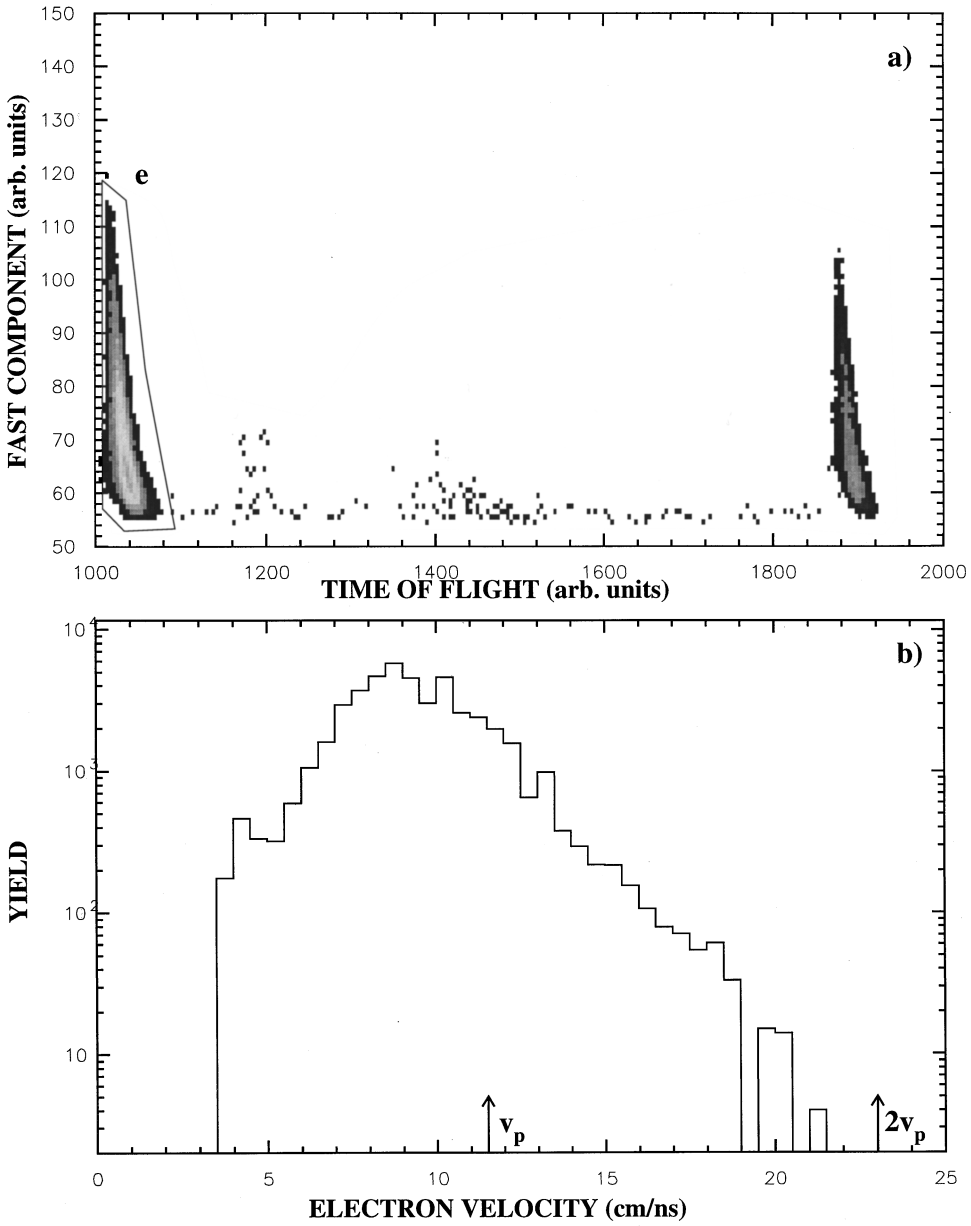

FIG. 2. (a) Fast component as a function of the time of flight for a backward-wall detector placed at 172°. The contour plot indicated by *e* has been used to select the electrons, whose velocity spectrum is shown in (b). The beam velocity ($v_P = 11.5$ cm/ns) and twice the beam velocity ($2v_P = 23$ cm/ns) are indicated in (b). Note also a second electron locus on the right-hand side of (a) due to the pulsed nature of the beam.

of 1.9 mm for the forward wall and variable thicknesses from 700 to 30 μm for the in-plane detectors and 30 μm for the backward wall. Full identification of all the reaction products is achieved by shape discrimination of the PM signals and time-of-flight techniques [15,16]. The PM signal consists of a fast and a slow component. The shape analysis is done by gating during two time windows with different widths; the output of the PM's and the two signals are charge integrated and digitized by QDC's. By plotting the fast versus the slow component, one can separate the different particles.

Electrons are well identified on the left line of Fig. 1(a), which corresponds to low-energy particles stopped in the plastic sheet. The other branch on the right is due to particles that do not interact with the plastic, but only with the cristal, such as direct γ rays, cosmic rays, and neutrons undergoing a nuclear reaction with the BaF_2 crystal. Figure 1(b) shows the fast component as a function of the time of flight for the electrons selected in the fast-slow representation [as indicated by the thin frame in Fig. 1(a)]. In Fig. 1(c) the deduced electron velocity spectrum is shown; the prompt γ-ray peak ($\Delta t \approx 500$ ps) has been taken as the reference time. The binary-encounter peak is well resolved, while threshold effects are important for lower velocities. The convoy electrons having velocities close to the beam velocities are very forward peaked and are not seen at this angle. The estimated resolution on the velocity measurement is $\Delta v/v \approx 5\%$.

In this experiment all the in-plane detectors, the backward wall, and only 14 out of 60 detectors of the forward wall were optimized for the detection of electrons by increasing the PM voltage. The other detectors of the forward wall

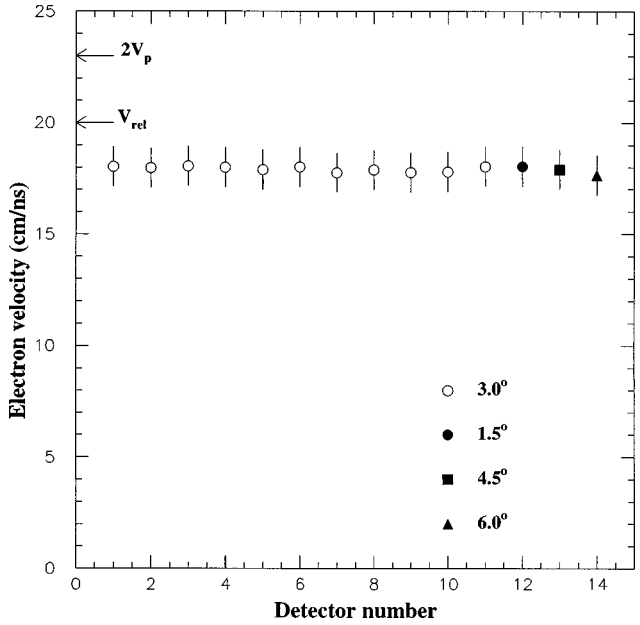

FIG. 3. Maximum position for the high-velocity component of the electron velocity spectra reported for 14 detectors of the forward wall at the indicated angles. The uncertainties of the measured velocity values are indicated by the error bars. The 0° expected electron velocities for a classical ($v_e = 2v_P$) and a relativistic [$v_e = v_{\rm rel}$ as given by formulas (1) and (2)] binary encounter, respectively, are also indicated.

worked in the usual way (''normal run''), i.e., detected charged nuclear products from light charged particles up to projectile fragments. A minimum multiplicity of 2 was required for an event to be recorded. We shall assume in the following that the detected electrons are uncorrelated with the coincident nuclear products or other detected particles, so their yield is a representative sample of the inclusive electron yield.

III. EXPERIMENTAL RESULTS AND COMPARISON TO THEORY

By using the experimental method outlined in the preceding section, we have extracted electron velocity spectra in the entire angular range, from 1.5° to 172°. For the forward angular range from 1.5° to 60°, the electronic threshold does not affect the high-velocity (BE) component of the spectrum, for which the maximum positions and relative cross sections can be extracted as a function of the laboratory angle unambiguously.

For angles greater than 60°, the threshold effects become significant on the velocity spectra. The extracted maximum positions must then be considered as an upper limit for the high-velocity component of the spectrum. As an example, the fast component is reported as a function of the time of flight in Fig. 2(a) for one of the backward-wall detectors at 172°. Although the fast component is truncated by the electronic threshold, there is evidence, by inspecting the two-dimensional plot, that a maximum lies above the threshold. Note also that a second electron locus is present on the right, due to the 81.5-ns radio-frequency repetition rate of the pulsed beam. The velocity spectrum, extracted following the contour plot *e* of Fig. 2(a), is reported in Fig. 2(b).

Figure 3 shows the maximum position for the electron velocity spectra measured in the 14 detectors of the forward wall, at the indicated angles. All the values are narrowly restricted around 18 cm/ns, somewhat lower than the 23 cm/ns expected if a classical binary encounter occurs between the incident ^{40}Ar ion of velocity $v_P = 11.5$ cm/ns and a pointlike electron at rest. Similar discrepancies are observed at other angles.

Plotted in Fig. 4 is the maximum position of the high-velocity component of the electron velocity spectrum as a function of the angle. Two features are clearly visible. First, from 1.5° to 60°, the maximum position behaves like $v_0 \cos\theta$, with $v_0 \approx 18$ cm/ns. This angular variation is expected from classical kinematics if a binary encounter occurs between the incident ^{40}Ar ion of velocity $v_P = 11.5$ cm/ns and a pointlike electron at rest. However, the v_0 value is somewhat lower than $2v_P = 23$ cm/ns, as predicted by this picture. Note that this $v_0 \approx 18$ cm/ns value is obtained independently for all of the 14 detectors of the forward wall.

Second, starting from 60° and for increasing angles, the behavior is almost flat at around 9.5 cm/ns. Taking into account the above discussion on the threshold effects, the position of the maximum at backward angles could be slightly overestimated, but there is in any case strong evidence for high-velocity electrons in the backward direction.

Recently, De Paola *et al.* [5] have introduced a billiard ball model including classical Rutherford scattering to repro-

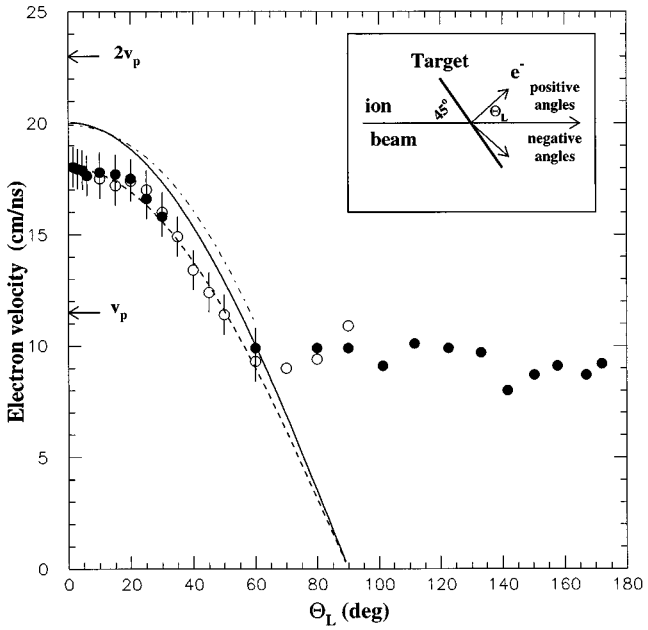

FIG. 4. Maximum position for the high-velocity component of the electron velocity spectra as a function of the laboratory angle. The uncertainties of the measured velocity values are indicated by the error bars for angles up to 60° that are not affected by threshold effects. The values for angles larger than 60° can be regarded as upper limits (see the text). The solid and the dot-dashed lines are the predictions of the billiard ball model [5] and the EIA calculations [6], respectively. The dashed line is the function $v = v_0 \cos\theta$, with $v_0 \approx 18$ cm/ns. The two arrows at 11.5 and 23 cm/ns indicate the beam velocity and twice the beam velocity, respectively. Empty and full circles are used for detectors placed at ''positive'' and ''negative'' angles with respect to the beam direction, respectively, as shown for clarity in the inset.

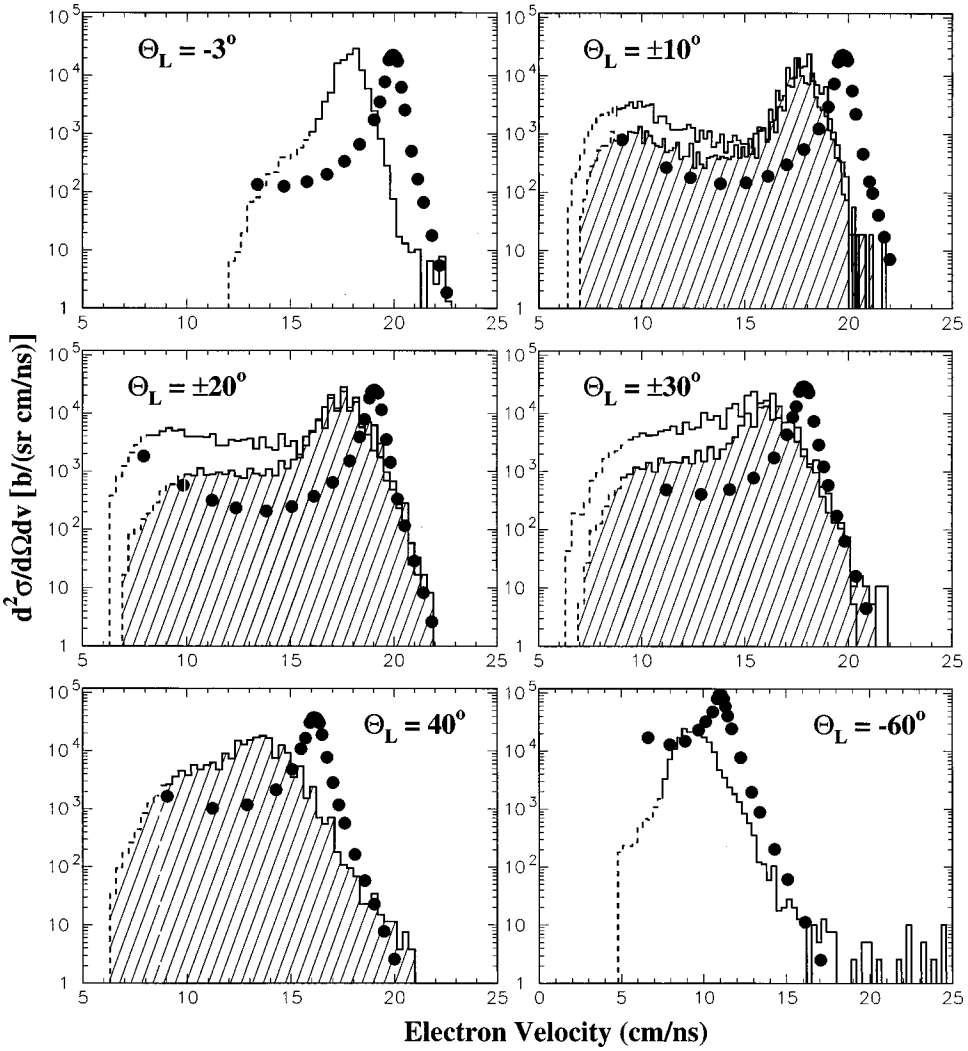

FIG. 5. Experimental electron velocity spectra [solid histograms (negative detection angles) and solid-hatched histograms (positive detection angles)] are compared with the spectra (in absolute units) as predicted by Ref. [6] (full circles) at the indicated laboratory angles. The maximum of the experimental spectrum at $-10°$ has been arbitrarily normalized to the maximum of the corresponding theoretical one. The part of the histogram affected by threshold effects is represented by a dashed line.

duce their relativistic data on binary-encounter electrons produced by bombarding a carbon foil with 35*A*- and 93*A*-MeV ^{40}Ar beams. In their experimental method a magnetic spectrometer was used to analyze the momentum of the electrons issued from the collision zone. They observe in general good agreement between the experimental data and the predictions of the model. We have reported the predictions of the billiard ball model [5] for the BE electron velocity as a function of the scattering angle in Fig. 4. The following formulas were used:

$$v_e(\text{cm/ns}) = c\,\frac{\sqrt{\dfrac{T_e}{m_e c^2}\left(2+\dfrac{T_e}{m_e c^2}\right)}}{1+\dfrac{T_e}{m_e c^2}} \qquad (1)$$

and

$$T_e(\text{MeV}) = \frac{2m_e c^2(T_p^2+2m_p c^2 T_p)\cos^2\theta_L}{E_T^2-(T_p^2+2m_p c^2 T_p)\cos^2\theta_L}, \qquad (2)$$

where $E_T = T_p + m_p c^2 + m_e c^2$, $c = 29.98$ cm/ns is the light velocity, $m_e c^2 = 0.511$ MeV and $m_p c^2$ are the electron and projectile rest mass, respectively, expressed in MeV, and T_e and T_p are the electron and projectile kinetic energy respectively, expressed in MeV. θ_L is the electron detection laboratory angle.

Note that the use of relativistic relations (1) reduces the classical v_0 value at 0° from 23 to 20 cm/ns. An overestimation of the maximum position still persists between 1.5° and 60°, where experimental values are approximately 10% lower than the predictions.

The double-differential cross sections $d^2\sigma/dv\,d\Omega$ are plotted in Fig. 5 for different emission angles θ_L as indicated. Note the difference between spectra for ''positive'' and ''negative'' angles from the tilted target (tilt angle 45° to the ion beam axis; see the inset in Fig. 4). Up to $\theta_L = 30°$, most of the electrons emitted in forward direction at negative angles must cross a larger effective target thickness than those emitted at positive angles. Only a small fraction of electrons stem from the outermost layers near the exit surface and leave the target without a secondary interaction and

form the high-energy part of the spectra. Therefore, the spectra for positive and negative angles agree well at high enough electron velocities (above and slightly below the BE peak maximum). In contrast, the spectra for negative angles show an enhanced intensity (up to a factor 3–5) in particular at low velocities. This is due to the contribution of secondary electrons created by fast electrons from deeper layers. At $\theta_L = \pm 30°$, the effective target thickness to be crossed by the fast electron at negative angles is up to about four times as large as for positive angles. Most of these electrons from deep within the solid have suffered secondary collisions and thus have lost a part of their initial velocity. From a simple estimate of the mean free path (MFP) of fast electrons in solids [which behaves like AE^n as a function of the electron energy, with material-dependent constants A and n as discussed in [7,10]] we can calculate that the target thickness of our Al target is in the order of four MFP's at 3° and 10°, so that the probability of secondary interaction is relatively small. In contrast, for negative angles at $\theta_L = 30°$, the effective target thickness increases to nearly 20 MFP's, so such transport effects (energy loss and angular straggling) cannot be neglected.

Let us now compare our experimental velocity spectra to the ones predicted by Ref. [6]. In these calculations (for details see Ref. [6]) the ejection of binary encounter electrons from the target by heavy, highly charged projectiles in a single collision is described by the quasielastic scattering approximation, where ionization takes place via electron transfer to the projectile continuum. At sufficiently energetic collisions, any interaction with the target core during the collision may be neglected [this is the so-called electron-impact approximation (EIA)]. The active electron scatters elastically from the projectile field and the corresponding cross section is then folded with the electron's momentum distribution in its initial state (the so-called Compton profile). In the numerical calculations, Hartree-Fock bound-state wave functions and experimental atomic binding energies were used. The influence of solid-state effects on the momentum distributions, particularly affecting the valence electrons, was not taken into consideration. Also, any thick target effects such as energy loss or angular straggling of the BE electrons on their way through the target have not been considered either.

The theoretical values (full circles in Fig. 5) have been convoluted to account for the experimental momentum resolution and normalized to the height of the experimental BE peak at $\theta_L = 10°$.

First of all, we observe that the experimental peaks are clearly shifted to lower energies at all angles. This result is surprising in view of the finding that experimental and theoretical BE peak positions are close for 35*A*- and 93*A*-MeV Ar impact on carbon foils [5].

Second, we observe that the shape and in particular the width of the experimental peaks are reasonably well reproduced by the calculation for the smallest ejection angles (3° and 10°). In this case, the widths are mainly determined by the initial momentum distribution of the bound target electrons (Compton profile) convoluted with the instrumental resolution since transport effects are of minor importance, as shown above. Even at the smallest angles, however, transport effects already broaden the experimental distribution with respect to theory.

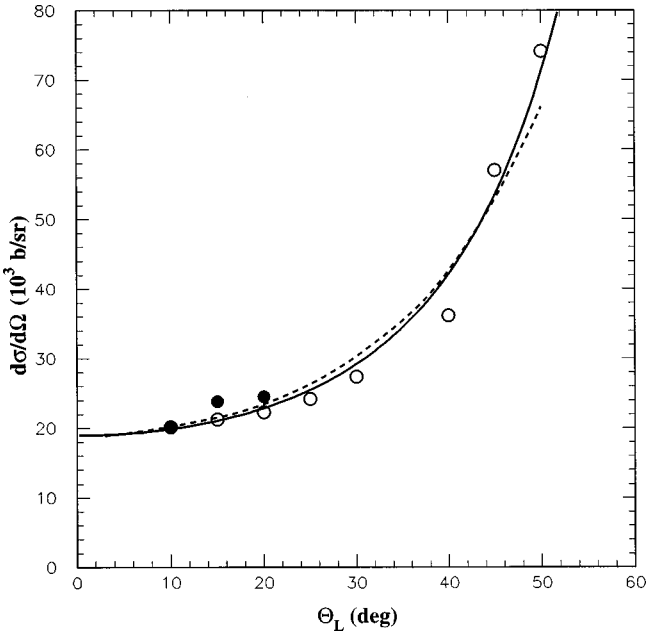

FIG. 6. High-velocity electron emission cross section as a function of the laboratory detection angle. The line represents the function const/$\cos^3 \theta_L$, as predicted in [5], while the dashed line is the prediction of calculations of Ref. [6]. Both experimental data and the predictions of [5] are normalized to the absolute value predicted by [6] at 10°. The symbols are the same as in Fig. 4.

Third, at larger angles, one clearly observes how the experimental peak becomes broader than the calculated peak, in particular for the negative angles spectra. As already discussed, this is due to secondary scattering of electrons in the solid. They suffer both angular scattering and energy loss on their way from the point of ionization to the surface. This broadens the distribution (angular and energy straggling) and shifts the maximum to lower velocities. Single collision conditions for the outgoing electrons are no longer fulfilled.

Finally, we find that the differential cross section as a function of the laboratory angle (see Fig. 6) shows a behavior compatible with a $1/\cos^3\theta_L$ law and is in agreement with the prediction of both the billiard ball model and the relativistic EIA [6].

IV. DISCUSSION AND CONCLUSION

The results of Fig. 4 need some further discussion and considerations before drawing some conclusions. First, the maximum of BE velocity spectra as a function of the laboratory angle is systematically smaller than the predictions of a simply relativistic two-body billiard ball model [5] and the more sophisticated EIA theory [6], unlike the experimental results of Ref. [5] (see above). We want to stress here that the experimental methods used here and in [5] are different. In fact, in Ref. [5] the use of a spectrometer is made, with connected calibration procedures, involving in particular the assumption that the electron cusp velocity is the same as the beam velocity. In our method we use the prompt γ-ray peak as reference time, measuring the γ-ray time of flight t_γ,

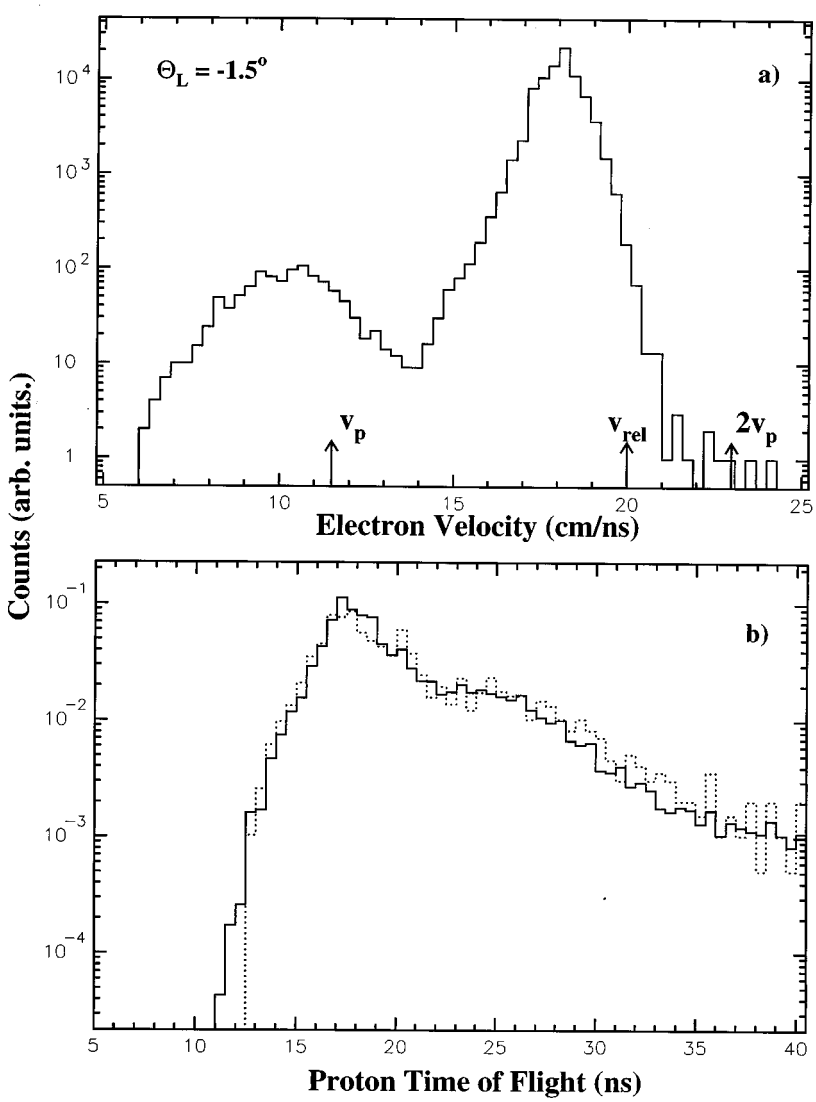

FIG. 7. (a) Experimental electron velocity spectrum for a forward-wall detector at $\theta_L = -1.5°$. The beam velocity ($v_P = 11.5$ cm/ns), twice the beam velocity ($2v_P = 23$ cm/ns), and the relativistic binary encounter velocity [$v_e = v_{\rm rel}$ as given by formulas (1) and (2)] are indicated. The first peak with a centroid close to the beam velocity is affected by threshold effects. The proton time-of-flight spectra are reported in (b) for the same detector as in (a) and for the same reaction ^{40}Ar(77*A* MeV) + ^{27}Al, respectively, for a run with ''normal'' (see the text) PM voltage in which the elastic peak relative to the reaction ^{40}Ar(77*A* MeV) + ^{197}Au has been taken as reference time (solid histogram) and for the run optimized for electron detection (present measurement), in which the prompt γ-ray peak has been taken as reference time (dashed histogram).

given by $t_\gamma = a(c_\gamma - c_0)$, where a (ns/channel) is obtained from the TDC (time to digital converter) calibration and c_γ is the measured prompt γ-ray peak centroid. We use then the extracted value of c_0 to convert the electron time of flight from c_e (TDC channels) to t_e (ns), as given by $t_e = a(c_e - c_0)$. We estimate the precision on the electron time of flight better than 1 ns. This leads to the estimated value of 18 cm/ns with an upper limit of 19 cm/ns for the BE electron velocity at the most forward angles, still below the value of 20 cm/ns predicted by [5].

A cross-check of our method is another calibration procedure, in which the c_0 parameter is calculated by taking another reference time, for instance, the one relative to the beam velocity. In a separate normal run (i.e., a run with normal gain of the PM in order to detect only nuclear products, disregarding γ and electron detection) we measured elastic scattering on a gold target and extracted the relative c_0 ($c_{0,\rm elast}$). We note that at our incident energy, we observed no ^{40}Ar elastic scattering on the Al target, even at the smallest detection angle $\theta_L = 1.5°$. We then constructed the proton velocity spectrum as shown in Fig. 7(b). On the other hand, by the same method as outlined above (see Fig. 1), we have separated electrons for this detector and obtained the electron velocity spectrum reported in Fig. 7(a), taking as reference the prompt γ-ray peak. This spectrum is dominated by the BE peak centered at approximately 18 cm/ns. We have also constructed the corresponding proton time-of-flight spectrum and compare it in Fig. 7(b) with the one obtained as described above by using the $c_{0,\rm elast}$ value. We find good agreement between the two time-of-flight spectra, either for this detector at $\theta_L = 1.5°$ and for the other 11 detectors of the forward wall at $\theta_L = 3°$. This is an important confirmation of the validity and precision of the method used.

We do not know the physical origin of the observed shift

of the electron velocity spectra with respect to the simple two-body picture of Ref. [5] and the EIA of Ref. [6]. Either the two models [5,6] are inadequate to describe the nucleus-electron interaction at these intermediate energies or other solid-state effects are present in the interaction between the incident ion and the atoms of the target. Experimental evidence has been reported for a deceleration of convoy electrons produced by 5*A*-MeV ions during the interaction with insulator foils [18], although such a mechanism seems unlikely in the present case of swift electrons that should have been ejected from the interaction zone before the ion track potential could have built up. Rather, two center effects and the complex dynamics of the electron in the combined projectile-target field [3] could be responsible for an energy shift. Another possibility lies in the influence of the projectile nucleus in the inverse kinematics of electron nucleus scattering at small impact parameters.

In conclusion, we have measured BE electron velocity spectra in a wide angular range by means of time-of-flight techniques. The main features of the data are nicely reproduced by the simple billiard ball model proposed in [5]. Also, the shape and in particular the width of the BE peak at small ejection angles are reasonably well reproduced by the EIA theory [6]. At larger angles, electron transport in the solid leads to a broadening of the measured peak. We observe, however, discrepancies as large as 10% between the experimental and the predicted electron emission velocities. A further result is an excess of energetic electrons in the backward direction, whose origin is not clear. Possible explanations include backscattering of electrons, which may be accounted for in the electron transport theories in solid targets [1,10,17]. To study this effect some experiments are planned [19], in which the electron velocity spectra will be measured as a function of the target thickness.

At the moment we cannot exclude *a priori* a nuclear origin for these electrons or for some of them, even if no studies exist to our knowledge to support this hypothesis. Nor can we exclude for the moment that the coincidence required between the electron and a projectilelike fragment in the forward direction, which automatically induces a correlation with the atomic impact parameters, favors the ejection of the most inner-shell atomic electrons. To elucidate this point, the analysis of the coincidence data together with the realization of more sophisticated coincidence experiments is planned for the future.

ACKNOWLEDGMENTS

We would like to thank the GANIL staff for providing a beam of excellent characteristics, J. Cacitti and C. Tribouillard from GANIL, Caen, and N. Giudice, N. Guardone, V. Sparti, and S. Urso from INFN, Catania for helping before and during the experiment. Useful discussions with R. Dayras are gratefully acknowledged.

[1] G. Schiwietz, in *Ionization of Solids by Heavy Particles*, edited by R. A. Baragiola (Plenum, New York, 1993); G. Schiwietz *et al.*, Phys. Rev. B **41**, 6262 (1990).

[2] H. Rothard, Scanning Microsc. **9**, 1 (1995).

[3] N. Stolterfoht, R. D. Dubois, and R. D. Rivarola, in *Electron Emission in Heavy-Ion-Atom Collision*, Springer Series on Atoms and Plasmas Vol. 20 (Springer, Berlin, 1997).

[4] H. Rothard, A. Billebaud, M. Jung, C. Caraby, B. Gervais, A. Cassimi, P. Jardin, R. Maier, M. Chevallier, J.-P. Grandin, and K. O. Groeneveld, Phys. Rev. A **51**, 3066 (1995); H. Rothard *et al.*, Nucl. Instrum. Methods Phys. Res. B **115**, 284 (1996).

[5] B. D. De Paola, Y. Kanai, P. Richard, Y. Nakai, T. Kambara, T. M. Kojima, and Y. Awaya, J. Phys. B **28**, 4283 (1995).

[6] D. H. Jakubassa-Amundsen, J. Phys. B **30**, 365 (1997).

[7] H. Rothard, D. H. Jakubassa-Amundsen, and A. Billebaud, J. Phys. B **31**, 1563 (1998).

[8] S. Suarez, R. O. Barrachina, and W. Meckbach, Phys. Rev. Lett. **77**, 474 (1996).

[9] U. Bechthold, S. Hagmann, J. Ullrich, B. Bathelt, A. Bohris, R. Moshammer, U. Ramm, C. Bhalla, G. Kraft, and H. Schmidt-Bocking, Phys. Rev. Lett. **79**, 2034 (1997).

[10] M. Jung, H. Rothard, B. Gervais, J.-P. Grandin, A. Clouvas, and R. Wunsch, Phys. Rev. A **54**, 4153 (1996).

[11] G. Lanzanò, E. De Filippo, and A. Pagano, in *Detectors for Nuclear Physics Experimental Activity at INFN Sezione di Catania*, Proceedings of the Workshop, Acireale (Catania), 1993, edited by S. Aiello, A. Palmeri, and F. Riggi (INFN, Catania, 1993), p. 10.

[12] G. Lanzanò, A. Pagano, E. De Filippo, E. Pollacco, R. Barth, B. Berthier, E. Berthoumieux, Y. Cassagnou, Sl. Cavallaro, J. L. Charvet, A. Cunsolo, R. Dayras, A. Foti, S. Harar, R. Legrain, V. Lips, C. Mazur, E. Norbeck, S. Urso, and C. Volant, Nucl. Instrum. Methods Phys. Res. A **323**, 694 (1992).

[13] E. De Filippo, R. Fonte, G. Lanzanò, and A. Pagano, Nuovo Cimento A **107**, 775 (1994).

[14] G. Lanzanò, E. De Filippo, M. Geraci, A. Pagano, S. Urso, N. Colonna, G. D'Erasmo, E. M. Fiore, and A. Pantaleo, Nuovo Cimento A **110**, 505 (1997), and references therein.

[15] G. Lanzanò, A. Pagano, S. Urso, E. De Filippo, B. Berthier, J. L. Charvet, R. Dayras, R. Legrain, R. Lucas, C. Mazur, E. Pollacco, J. E. Sauvestre, C. Volant, C. Beck, B. Djerroud, and B. Heusch, Nucl. Instrum. Methods Phys. Res. A **312**, 515 (1992).

[16] G. Lanzanò, E. De Filippo, M. Geraci, A. Pagano, S. Aiello, A. Cunsolo, R. Fonte, A. Foti, M. L. Sperduto, C. Volant, J. L. Charvet, R. Dayras, and R. Legrain, in *Proceedings of the XXXV International Winter Meeting on Nuclear Physics, Bormio, 1997*, edited by I. Iori (Università di Milano, Milano, 1997), p. 536.

[17] R. A. Sparrow, R. E. Olson, and D. Schneider, J. Phys. B **25**, L295 (1992).

[18] G. Xiao, G. Schiwietz, P. L. Grande, N. Stolterfoht, A. Schmoldt, M. Grether, R. Kohrbruck, A. Spieler, and U. Stettner, Phys. Rev. Lett. **79**, 1821 (1997).

[19] G. Lanzanò, H. Rothard, S. Aiello, E. De Filippo, M. Geraci, A. Pagano, G. Politi, A. Anzalone, S. Cavallaro, D. Mahboub, B. Gervais, M. M. Meier, J. U. Schott, and D. H. Jakubassa-Amundsen (unpublished).